Flexible and robust silicon/carbon nanotube anodes exhibiting high areal capacities

Chong Xie [a], Na Xu [a], Peiyi Shi [a], Yixuan Lv [b], Hirbod Maleki Kheimeh Sari [a], Jian-Wen Shi [b,*], Wei Xiao [a], Jian Qin [a], Huijuan Yang [a], Wenbin Li [a], Jingjing Wang [a], Junhua Hu [c], Xueliang Sun [a,d,*], Xifei Li [a,*]

[a] Xi'an Key Laboratory of New Energy Materials and Devices, Institute of Advanced Electrochemical Energy, School of Materials Science and Engineering, Xi'an University of Technology, Xi'an, Shaanxi 710048, China
[b] State Key Laboratory of Electrical Insulation and Power Equipment, Center of Nanomaterials for Renewable Energy, School of Electrical Engineering, Xi'an Jiaotong University, Xi'an 710049, China
[c] Center for International Cooperation on Designer Low-carbon & Environmental Materials (CDLCEM), Zhengzhou University, Zhengzhou, Henan 450001, China
[d] Department of Mechanical & Materials Engineering, University of Western Ontario, London, Ontario N6A 5B9, Canada

GRAPHICAL ABSTRACT
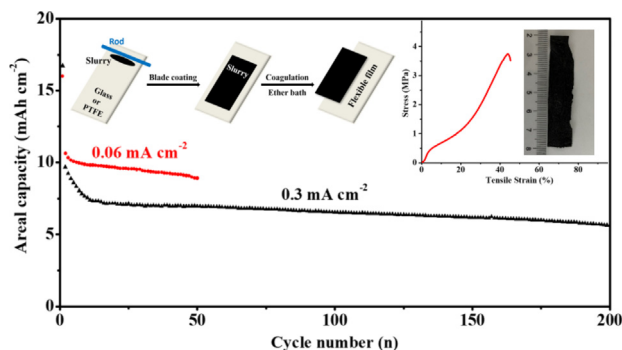
ARTICLE INFO

ABSTRACT

The fast development of flexible devices has greatly boosted the demands for flexible lithium-ion batteries (LIBs). Accordingly, a broad exploration of flexible electrodes in LIBs is crucial. At present, the major challenge in the flexible electrode for lithium-ion batteries (LIBs) is how to achieve an excellent electrochemical performance (particularly high-energy density) while maintaining superior mechanical flexibility. Herein, flexible silicon/carbon nanotube (Si/CNT) electrode is prepared via a common blade-coating, which is adoptable to large-scale production. The CNT network from monodispersed CNT solution endows the electrode with superior tensile strength and mechanical toughness. The tensile strength of the flexible electrodes is up to 3.75 MPa, and the corresponding strain at break is 43.9%. The flexible electrode delivers an areal capacity of 10.6 mAh cm^{-2} at 0.06 mA cm^{-2}, which is completely meet the practical requirement (1–3 mAh cm^{-2}). And a high reversible capacity of 5.64 mAh cm^{-2} can be retained at 0.3 mA cm^{-2} after 200 cycles. In addition, the pouch cell exhibits a promising cycling stability under the repeated deformation state. Moreover, this work also provides a feasible and scalable method to fabricate flexible electrodes for other wearable energy storage systems.

© 2022 Elsevier Inc. All rights reserved.

* Corresponding authors at: No.5, South Jinhua Road, Xi'an 710048, Shaanxi, China.
  E-mail addresses: jianwen.shi@xjtu.edu.cn (J.-W. Shi), xsun9@uwo.ca (X. Sun), xfli2011@hotmail.com (X. Li).

1. Introduction

Recently, wearable electronic devices have become as fundamental features in one's daily life. LIBs are considered as one of the best candidates for the power source of such devices. However, traditional LIBs are heavy and rigid, which hardly meet the power requirements of these electronic devices. Consequently, it is necessary to explore a new-generation LIBs with flexible, lightweight and stretchable to satisfy the power demands of such devices. As a core component of LIBs, the explore of flexible electrode is crucial [1–3].

During the past decade, remarkable achievements have been accomplished in the development of flexible electrodes. Carbon nanomaterials, such as carbon nanotube (CNT), graphene etc., with excellent electrical conductivity and mechanical properties, are considered to be one of the best candidates for fabricating flexible electrodes. Regarding the structure, flexible electrodes have two different categories: paper-supported electrode and paper-like electrode [4]. In case of the former, the slurry (active materials) is coated on flexible carbon paper, which is worked as the current collector. However, the poor adhesion between the slurry and carbon paper directly decreases the mechanical and electrical contact. As a result, the active material layer easily falls off the surface of the current collector, especially when being bent or folded [1]. Thus, the paper-supported electrode exhibits moderate cycling performance. On the other hand, paper-like electrode could avoid such issues. In this electrode, active material is embedded in the interior. The carbon matrix provides both mechanical support and conductive network [4]. At present, the common method of preparing paper-like electrode is vacuum filtration, which is time-consuming and barely scale-up [5–8]. And the sluggish filtration process also leads to the uneven distribution of the active materials in the interior, especially for thicker electrode. Meanwhile, the mechanical toughness of such electrodes rapidly deteriorates with large thickness and high mass loading of active materials [1]. Therefore, it is still a challenge to develop a simple method for producing the thicker paper-like electrodes with promising electrochemical performance and mechanical strength on a large scale.

Silicon (Si)-based materials with the high theoretical specific capacity (3579 mAh g^{-1} for $Li_{3.75}Si$) are considered to be one of the most promising LIB anodes [9–14]. Si-based materials used as the active materials of flexible electrodes could deliver a high energy density. However, huge volume variation of Si during the electrochemical process deteriorates the structural integrity of electrodes, resulting in the rapid capacity fading [15]. Therefore, matrix of the flexible electrodes should possess mechanically robust and flexible structure to alleviate the volume variation of Si and maintain the structural stability.

Based on these considerations above, herein, simple blade-coating method has been explored to fabricate the thicker paper-like electrodes. Among them, CNTs are the flexible matrix, and carbon coated Si nanoparticles (Si@C) are the active materials. These flexible electrodes (Si@C-CNTs) have several advantages. First, CNT network from monodispersed CNT solution [16–20] with an impressive mechanical property perfectly ensures the structural integrity of the flexible electrode during the electrochemical process. Second, the porous structure formed by the entangled CNTs could not only provide fast channels for Li-ion transportation, but also alleviate the volume expansion of Si nanoparticles. Third, the presence of carbon coating layer on Si nanoparticles could suppress volume expansion of Si nanoparticles, and also effectively improve the electrical contact between CNTs and Si nanoparticles. Fourth, the thickness of flexible electrode is more than 100 μm, and

this preparation method is easy and adoptable to large-scale production. As excepted, the flexible electrode demonstrates a high areal capacity of 10.6 mAh cm^{-2} at 0.06 mA cm^{-2}, and a reversible capacity of 5.64 mAh cm^{-2} at 0.3 mA cm^{-2} after 200 cycles. Additionally, the tensile strength of the flexible electrode is as high as 3.75 MPa, and the corresponding strain at break (elongation) is 43.9%.

2. Experimental

2.1. Preparation of flexible electrodes

2.1.1. Preparation of Si@C nanoparticles

60 mg Si nanoparticles (Alfa Aesar) were uniformly dispersed in a solution of 14 mL C_2H_5OH and 40 mL H_2O by ultrasonication. Then, 50 mg CTAB ($C_{19}H_{42}BrN$) was added into the above dispersion. After reaction for 15 min, 60 μL ammonia, 15 mg resorcinol and 28 μL formaldehyde were introduced successively. After stirring for 24 h at room temperature, Si@RF could be obtained via filtration. Finally, the Si@RF nanocomposites were carbonized at 800 °C under Ar for 3 h to prepare the Si@C.

2.1.2. Preparation of flexible electrodes

The preparation of CNTs was referred to our previous work [18,19]. Blade-coating was chosen to fabricate the flexible film. Firstly, CNTs were evenly dispersed in the chlorosulfonic acid (CSA). And the mass fraction of the CNTs in the dispersion is 0.8–1.2 wt%. Then Si@C nanoparticles with a certain content were introduced into the above mixture. After stirring fiercely, the slurry can be obtained. Afterwards, the slurry was uniformly coated onto a piece of glass matrix. After coagulation in ether solution for 20 min, the flexible film could be obtained after washing with H_2O and drying at 110 °C for 12 h. The contents of Si@C in the electrodes were regulated by varying the ratios of Si@C to CNTs in the slurry. In this work, the mass ratios of Si@C nanoparticles to CNTs are 1:1, 2:1 and 3:1, and the corresponding electrodes are denoted as Si@C-CNTs, 2Si@C-CNTs and 3Si@C-CNTs, respectively. Therefore, the Si@C mass loadings for Si@C-CNTs, 2Si@C-CNTs and 3Si@C-CNTs are 50 wt%, 67 wt% and 75 wt%, respectively.

The Characterization and the Electrochemical Measurement are in the Supporting Information.

3. Results and discussion

In this work, the CNTs were synthesized by CVD method. After purification, CNTs with high quality could be obtained. The CNTs are mainly double-walled carbon nanotubes (DWCNTs) (Figure S1a), which also contain a small amount of single-walled carbon nanotubes (SWCNTs) and triple-walled carbon nanotubes (TWCNTs). According to the Raman spectrum of purified CNTs (Figure S1b), several little peaks below 300 cm^{-1} are the radial-breathing-modes (RBM) peaks [21], which are the typical characteristics of small-diameter CNTs (Figure S1a). In addition, there is no visible D-band in the Raman spectrum, evidently indicating the perfect structure of CNTs. High-quality CNTs, especially high purity and large aspect ratio, help to endow the flexible films with superior electrical and mechanical performance [17,22].

Fig. 1a exhibits the route for making flexible electrodes by the common blade-coating method. The CNTs were independently dispersed in CSA without the use of any other surfactants, which is the only known CNT solvent. Subsequently, the active materials (Si@C nanoparticles) were uniformly dispersed in CNT solution using a high-speed mixer to obtain the slurry (Fig. 1b). Achieving uniform distribution of CNTs and active materials, and consequently homo-
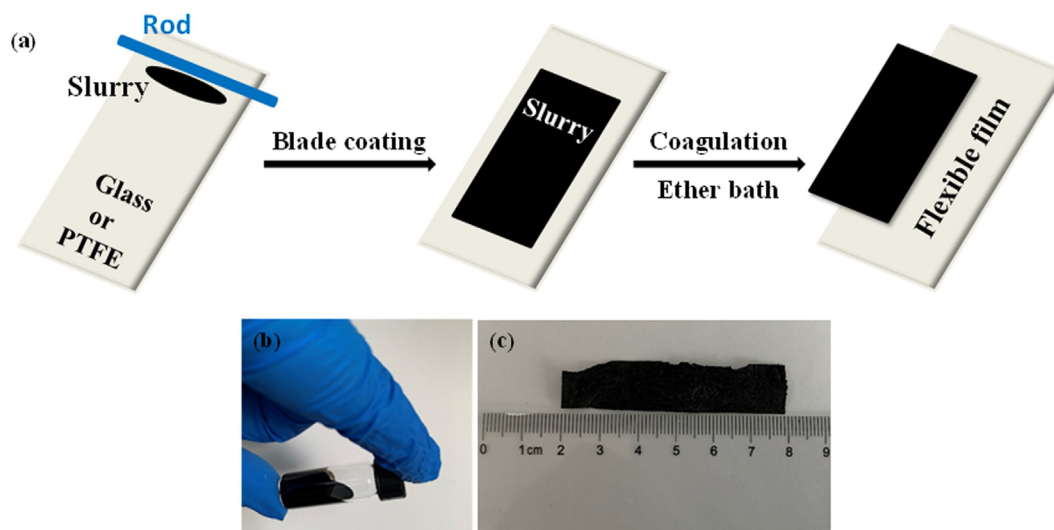
Fig. 1. (a) Schematic illustration of the route for preparing the flexible films; (b) The slurry; (c) The photograph of pristine flexible electrode.

geneous slurry is the key to obtaining flexible films with superior electrical and mechanical performance. The better the dispersion of slurry, the better the property of flexible electrode [5]. According to our experience, only the slurry with suitable viscosity can be processed into an intact and uniform film, and the optimal content range of CNTs and active materials in slurry is 1.5 to 3 wt%. The monodispersed CNTs assemble into CNT bundles via the intermolecular force during the solidification process, and then form macroscopic dense CNT film. At the same time, the active materials (Si@C) are immobilized in the film. After coagulation in ether bath for 30 min, an intact flexible film could be obtained (Fig. 1c). The entire fabrication routine is easy and suitable for industrial production. And note that there are no conductive additives or binders in the flexible film, which do not contribute to capacity, but lower the energy density of the whole electrode.

Applying Si/C nanocomposites with core-shell structure is one promising approach to improve the electrochemical performance of Si-based anodes [23]. Fig. 2a and b demonstrate the TEM images of Si@C nanoparticles, which have a diameter range of 30–120 nm. As shown in Fig. 2b, an amorphous carbon layer with a thickness of about 3–4 nm has been evenly coated on the surface of Si nanoparticle with high crystallinity. And according to the TGA curve (Figure S2), the mass fraction of carbon in the Si@C nanoparticles is about 5 wt%. Therefore, the mass fractions of Si in the flexible Si@C-CNTs, 2Si@C-CNTs and 3Si@C-CNTs electrodes are 47.5 wt%, 63.3 wt% and 71.3 wt%, respectively. Carbon layer can not only suppress volume expansion of Si nanoparticle, but also enhance the electrical contact between CNTs and Si nanoparticles, leading to the improved electrochemical performance [23]. Fig. 2c-e also exhibit SEM images of the flexible electrodes. As displayed in Fig. 2c, no obvious Si@C clusters can be observed in Si@C-CNTs electrode. Si@C nanoparticles are distributed uniformly in CNT network, guaranteeing the electrochemical activity of every Si@C nanoparticle. Meanwhile, the dense network constructed by entangled CNT bundles not only supplies channels for lithium ion transportation, but also provides buffer space for Si@C during the electrochemical process. Unfortunately, as the Si@C mass loading gradually increases, some Si@C clusters appear in the electrode (Fig. 2d and e, Figure S3). Since there are no binders among Si@C nanoparticles in the clusters, which easily rupture during the electrochemical process, resulting in the worse electrical contacts and rapid capacity fading. Meanwhile, a high Si@C mass loading would damage the mechanical properties as a crucial parameter for the

flexible electrode, along with the electrochemical performance. Hence when designing flexible electrodes, the electrochemical performance and mechanical property should be considered comprehensively. On the other hand, as there are no polymer binders or surfactants used during the routine of preparing the flexible electrodes, the strong cohesion between monodispersed CNTs bundles ensures the superior mechanical toughness of the CNT matrix. As shown in Fig. 2f, the flexible electrode can be twisted at any angle, indicating the superior mechanical flexibility of the as-prepared electrode, which is also beneficial to the improved electrochemical performance. Fig. 2g-i exhibit the SEM images of the cross-section of the flexible electrodes. The average thickness of Si@C-CNTs, 2Si@C-CNTs and 3Si@C-CNTs electrodes are about 84, 130 and 150 µm, respectively. The insert on the right in Fig. 2h demonstrates that the Si@C nanoparticles are distributed uniformly in the flexible electrode.

XRD and Raman patterns were tested to analyse the structural properties of the samples. As shown in Fig. 3a, all of the diffraction peaks belong to the crystalline Si [24]. After the carbon layer coating, intensities of the peaks slightly decrease. Due to the fact that the thickness of amorphous carbon layer is only several nanometres (Fig. 2b), no reflected peaks belong to this layer can be observed. Figure S4 shows XRD pattern of the resulting flexible electrode. As shown in Figure S4, XRD pattern of the flexible electrodes is similar with that of the Si@C nanoparticles, except a broad diffraction peak from CNTs. These results indicate that the morphology of Si nanoparticles remains unchanged during the synthetic process. Indeed, Raman spectroscopy is a more effective approach to analyse the carbon-based materials [25]. For pure Si nanoparticles, two peaks around 520 and 920 cm^{-1} are attributed to the phonon scatterings of crystalline Si [26]. In addition, G-band and D-band could be conspicuously observed in the Raman spectra of Si@C nanoparticles (Fig. 3b), suggesting the existence of an amorphous carbon layer. Fig. 3c exhibits Raman spectra of the flexible electrodes. Due to the strong scattering of CNTs, only a tiny peak around 520 cm^{-1} emerges in the entire Raman spectra, and whose intensity increases with the mass loading increase of Si@C nanoparticles.

The electrochemical performances of all flexible films were investigated as LIB anodes. Figure S5a exhibits the cycle performances of Si and Si@C nanoparticles coated on copper foil. After 100 cycles, the capacity retention of Si@C electrode was 58%, which was much better than that (7.7%) of the pure Si electrode. Evi-
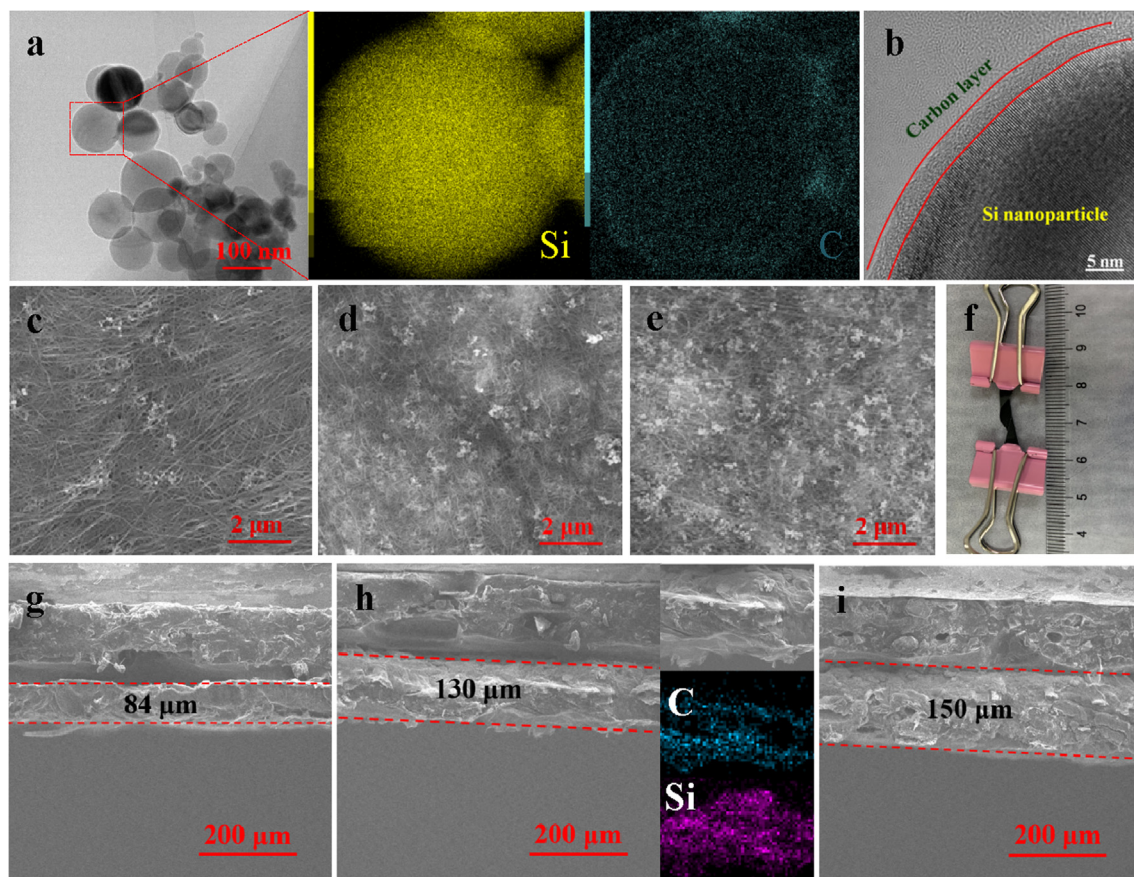
Fig. 2. (a) TEM image and corresponding elemental mapping of Si@C nanoparticle; (b) HR-TEM image of Si@C nanoparticle; SEM images of the flexible electrodes (c) Si@C-CNTs, (d) 2Si@C-CNTs and (e) 3Si@C-CNTs; (f) A photograph of twisted flexible electrode; SEM images of the cross-section of flexible electrodes (g) Si@C-CNTs, (h) 2Si@C-CNTs (the inset on the right shows the elemental mapping), and (i) 3Si@C-CNTs.
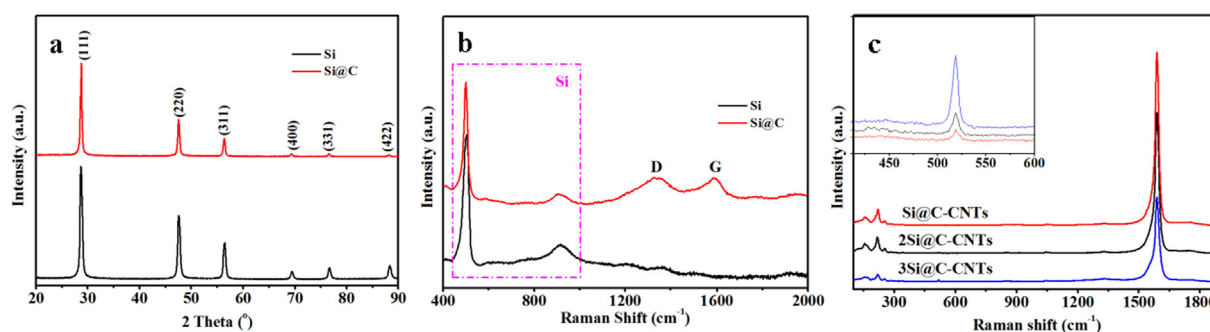

Fig. 3. (a) XRD and (b) Raman patterns of pure Si and Si@C nanoparticles; (c) Raman spectra of the flexible electrodes.

dently, the cycling stability of Si nanoparticles is significantly improved after carbon coating. Both Si and Si@C are also used as active materials to prepare the flexible electrodes, and the ratio of active materials and CNTs is 1:1. Compared with the Si-CNTs flexible electrode, Si@C-CNTs exhibits a better cycling stability (Figure S5b). In this work, the specific capacities of the flexible electrodes were calculated based on the total mass of Si@C nanoparticles and CNT matrix, even though CNT matrix made negligible contribution to the capacity (Figure S5c).

Fig. 4a makes a comparison among the cyclic stability of the flexible electrodes at 0.1 A g^{-1} with different Si@C mass loading. As the Si@C mass loading increases in CNT network, the cycle stability of the flexible electrodes gradually decreases. Si@C-CNTs and 2Si@C-CNTs deliver reversible capacities of 1237 mAh g^{-1} and

1551 mAh g^{-1} after 50 cycles, respectively, with the corresponding capacity retentions are 88.7% and 83.9%. However, the reversible capacity of 3Si@C-CNTs is less than 1000 mAh g^{-1} after 35 cycles. When the current density is increased to 0.5 A g^{-1}, Si@C-CNTs, 2Si@C-CNTs and 3Si@C-CNTs electrodes deliver reversible capacities of 803, 1140 and 458 mAh g^{-1} after 100 cycles, respectively. Taking into account both cycling stability and specific capacity, the 2Si@C-CNTs electrode exhibits a superior electrochemical performance among the three electrodes. For 2Si@C-CNTs electrode, the reversible capacity is still close to 1000 mAh g^{-1} after 200 cycles, and the capacity retention is 79.2% from the 20th to the 200th cycle (Figure S6). The rapid capacity fading during the first 20 cycles could be attributed to the pulverization of Si@C clusters in the CNT network (Fig. 2d and S7). The superior cycling stability
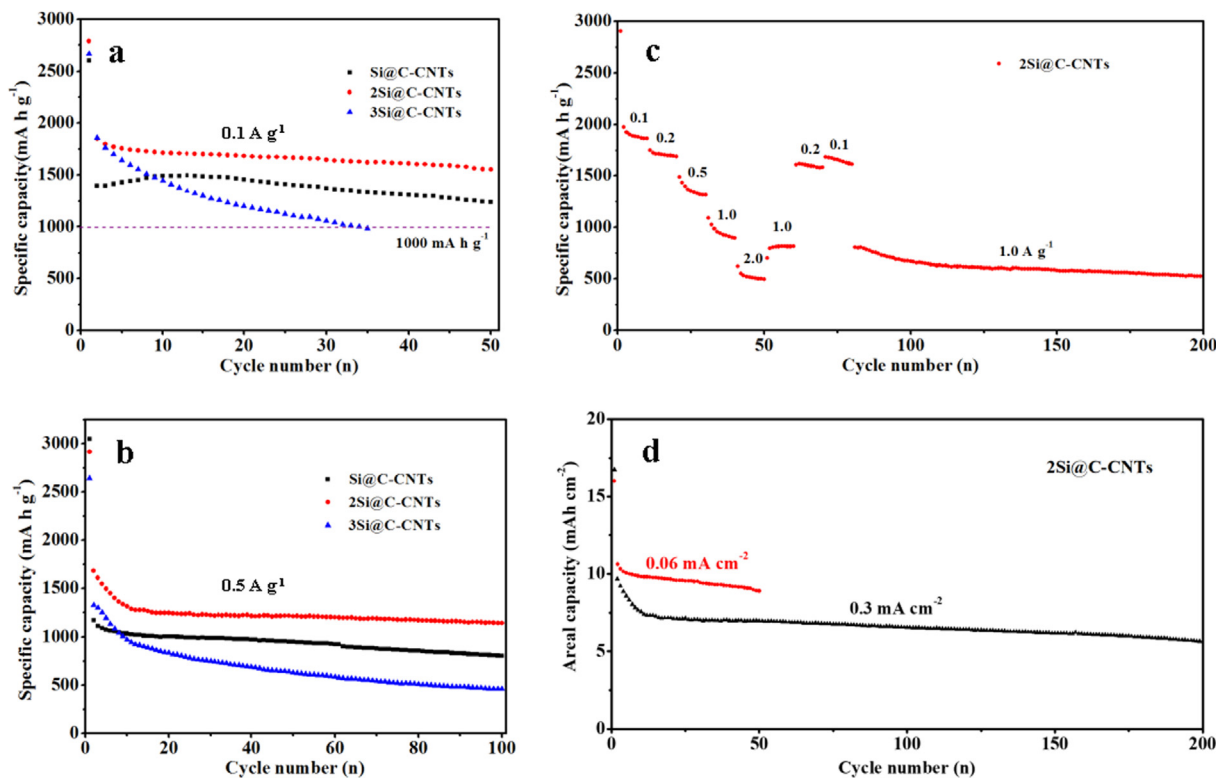
Fig. 4. Cycle performances of the flexible electrodes at (a) 0.1 A g^{-1} and (b) 0.5 A g^{-1}; (c) Rate performance of 2Si@C-CNTs electrode at different current densities; The specific capacities of flexible electrodes were calculated based on the mass of Si@C nanoparticles and CNT matrix. (d) The areal capacity of 2Si@C-CNTs electrode.

for the rest cycles is attributed to the robust mechanical strength of CNT matrix. The stress caused by the volume variation of Si during the electrochemical process could be transferred among the CNT-CNT bundles [27]. Fig. 4c shows the rate performance of 2Si@C-CNTs and long cycle performance at 1.0 A g^{-1}. Due to the porous structure of CNT network, a specific capacity of 621 mAh g^{-1} can be maintained at current density of 2.0 A g^{-1}. Note that the thickness of the 2Si@C-CNTs electrode is up to 130 μm, the rate performance of the flexible electrode is competitive. The areal capacities of 2Si@C-CNTs electrode were also calculated (Fig. 4d). The maximum areal capacity reaches 10.6 mAh cm^{-2} at the current density of 0.06 mA cm^{-2}, and it is still as high as 8.9 mAh cm^{-2} after 50 cycles, which is completely meet the practical requirement (1–3 mAh cm^{-2}) [28]. The flexible electrode also delivers a high areal capacity of 5.64 mAh cm^{-2} at 0.3 mA cm^{-2} after 200 cycles. More importantly, the capacity is calculated based on the mass of whole electrode, and there are no metallic current collectors (inert component) in the electrodes. Undoubtedly, the designed flexible electrodes are effective on enhancing the device's gravimetric energy density of LIBs.

Since the 2Si@C-CNTs electrode exhibits the best comprehensive electrochemical performance among the tested electrodes, which was chosen for studying the lithium storage kinetics of flexible electrode. Fig. 5a shows the cyclic voltammetry (CV) curves of the 2Si@C-CNTs electrode under different scan rates. The wide cathodic peak around 0.2 V during the lithiation process is ascribable to the formation of Li$_x$Si alloy. And the two anodic peaks around 0.34 V and 0.53 V during the delithiation process are caused by the conversion of Li$_x$Si to Si [29]. The peak currents at different scan rates can be used to assess the diffusion-controlled electrochemical process. Generally, the relationship between the scan rate (v) and peak current (i) can be expressed as $i = av^b$, where a and b are adjustable values. If the b-value is 1, indicating the capacity dominated by surface reaction. If the b-value is 0.5, sug-

gesting the capacity controlled by solid-state diffusion [30,31]. For the 2Si@C-CNTs electrode, the b-value is 0.56, indicating that the capacity is determined by solid-state diffusion, i.e. phase transformation of Si nanoparticles. Fig. 5c exhibits the Nyquist plots of the 2Si@C-CNTs electrode after different cycles. The impedance spectra consist of two semi-circle loops and a linear tail. Fig. 5d and S8 exhibit the fitted curves according to the equivalent circuit. R_s is the total Ohmic resistance of electrodes, electrolyte and separator in the battery, corresponding to the intercept in the high frequency region on the x-axis [32]. R_f and R_{ct} are the resistance from the Li ions through the SEI layer and the charge transfer resistance, respectively. CPE$_1$ and CPE$_2$ are the capacitance of the SEI layer and the double-layer capacitance, respectively. W is the Warburg diffusion element, corresponding to the straight line towards the end of the curve, related to a combined effect of Li ions diffusion across the electrode-electrolyte interfaces [33]. The low Ohmic resistance (R_s) is attributed to the excellent electrical conductivity of CNT networks. The slight increase of R_f and R_{ct} resistance during the cycling process is due to the ageing of the electrodes and the growth of SEI layer. The slope of W is almost parallel to the real axis, indicating that the electrodes show the characteristic of a high-quality supercapacitor because of CNT networks [34].

Besides the electrochemical performance, the mechanical strength of the flexible electrodes should not be neglected. Hence, the tensile test was carried out to measure the mechanical properties of flexible electrodes. Fig. 6a shows the tensile stress-strain curves of flexible electrodes. According to the shape of tensile stress-strain curves, the fracture mechanism of all flexible electrodes is brittle fracture. Figure S9 exhibits the photograph of the 2Si@C-CNTs flexible electrode after tensile test. As the mass loading of Si@C nanoparticles in CNTs network increases, the tensile strength of the flexible electrode gradually decreases. The tensile strengths of Si@C-CNTs, 2Si@C-CNTs and 3Si@C-CNTs are 4.00, 3.75 and 2.66 MPa, respectively, which are at least an order of mag-
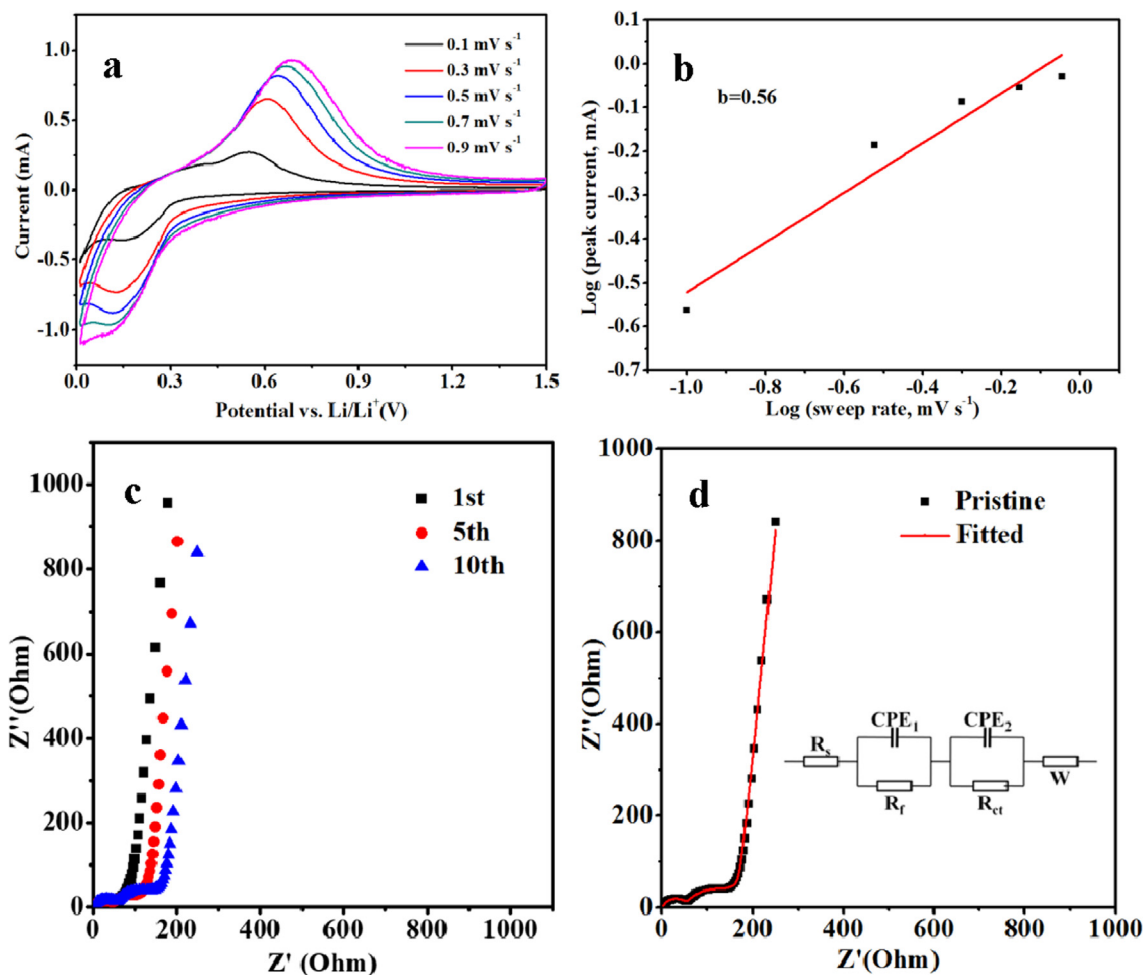
Fig. 5. (a) CV curves of the 2Si@C-CNTs electrode from 0.1 to 0.9 mV s^{-1}; (b) b-value determination of the peak currents from anodic peaks; (c) Nyquist plots of the 2Si@C-CNTs electrode (charge state); (d) Nyquist plot and fitted curve of the 2Si@C-CNTs electrode after 10 cycles, and insert is the equivalent circuit.
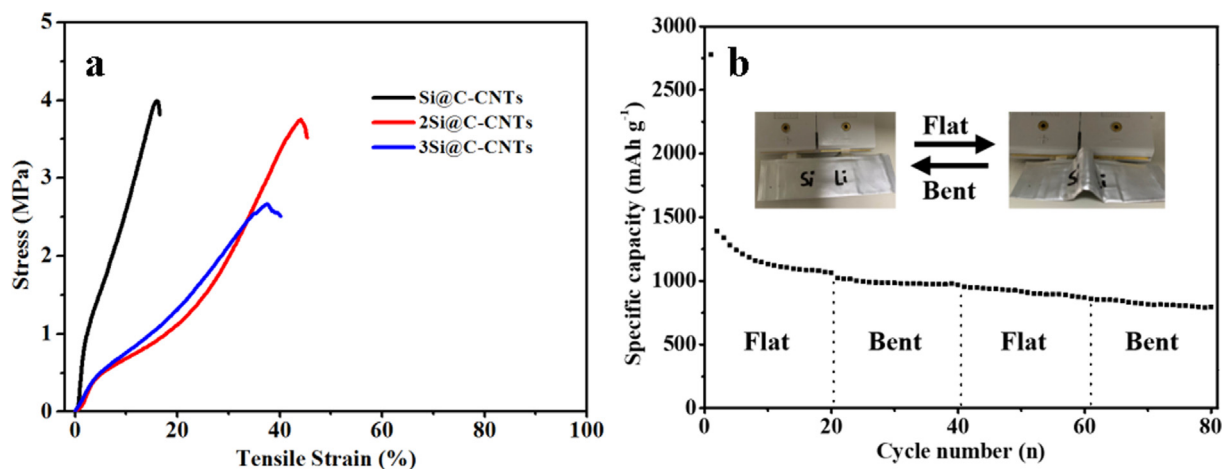

Fig. 6. (a) Tensile stress-strain curves of flexible electrodes; (b) The cyclic stability of the pouch cell under repeated deformation state at 0.5 A g^{-1}.

nitude higher than those of conventional electrodes [35]. And the corresponding strains at break (elongations) are 15.8%, 43.9% and 37.6%, respectively. The high tensile strength and large elongation make the electrode resistant to mechanical fatigue and fracture, ensuring the structural integrity during the (de)lithiation process and distortion. The excellent mechanical properties of the flexible

electrodes are attributed to uniform slurry, particularly the monodispersed CNT with high purity and large aspect ratio, which is the key to strength improvements [17,27].

In most of the flexible electrodes reported before, the flexibility is presented by showing the photo of folded, bended or twisted electrodes. Only a few articles test the mechanical strength of Si-

based flexible electrodes, whose tensile strengths (below 1.0 MPa) are much lower than that of our flexible electrode (Table S1) [8,36]. On the other hand, the specific capacities of most electrodes are solely calculated based on the mass of active materials, which makes it difficult to directly compare the obtained data with other Si-based flexible electrodes. The specific capacity and areal capacity of our flexible electrode are 1851.7 mAh g^{-1} and 10.6 mAh cm^{-2}, respectively. The areal capacity is much higher than those of other flexible Si-based anodes pubilished before. For example, a flexible Si-based anode with a high areal capacity (5.58 mAh cm^{-2}) has been reported by Cui et al. [37]. Even compared with other Si-based electrodes coated on Cu foil, the areal capacity and cycle stability of the prepared flexible electrode in this study is still competitive (Table S1) [38,39].

To further study the practical application of the flexible electrodes in the wearable electronics, the 2Si@C-CNTs electrode was chosen as the working electrode to assemble the pouch type half cell. As shown in Fig. 6b, due to the Si@C clusters in the 2Si@C-CNTs electrode, the pouch cell also demonstrates rapid capacity fading under the flat state during the first 20 cycles. After the subsequent 60 cycles, the pouch cell shows a promising cycling stability under the repeated deformation, and the capacity retention is 77.6 % from the 21th to the 80th cycle. The corresponding specific capacity of the pouch cell at the 80th cycle is 793 mAh g^{-1}. Obviously, the robust mechanical strength and large elongation of the flexible electrodes hold the cycling stability under the repeated deformation state (Fig. 2f and 6), indicating the great potential for applying the electrodes in flexible LIBs. Furthermore, the manufacturing routine of the flexible electrodes is simple and suitable for implementing in industrial production.

4. Conclusions

In summary, fleixbile Si-based electrodes for LIB anodes were prepared via blade-coating technique. This approach is easy to implement in industrial production. The flexible electrodes achieve an impressive combination of electrochemical performance and mechanical strength. The areal capacity is as high as 10.6 mAh cm^{-2} at 0.06 mA cm^{-2}, and the tensile strength of the flexible electrode is up to 3.75 MPa with 43.9% strain. In addition, the fabrication approach is also applicable to prepare other energy storage systems, such as lithium-sulfur battery (LSB), sodium-ion battery (SIB) and potassium-ion battery (PIB) electrodes, etc.

CRediT authorship contribution statement

Chong Xie: Conceptualization, Methodology, Investigation, Formal analysis, Writing – original draft. **Na Xu:** Investigation, Formal analysis. **Peiyi Shi:** Investigation. **Yixuan Lv:** Investigation. **Hirbod Maleki Kheimeh Sari:** . **Jian-wen Shi:** Investigation. **Wei Xiao:** . **Jian Qin:** . **Huijuan Yang:** . **Wenbin Li:** Resources. **Jingjing Wang:** Resources. **Junhua Hu:** . **Xueliang Sun:** Writing – review & editing. **Xifei Li:** Supervision, Writing – review & editing.

Declaration of Competing Interest

The authors declare that they have no known competing financial interests or personal relationships that could have appeared to influence the work reported in this paper.

Acknowledgements

Appendix A. Supplementary data

Supplementary data to this article can be found online at https://doi.org/10.1016/j.jcis.2022.06.082.

References

[1] Z. Wu, Y. Wang, X. Liu, C. Lv, Y. Li, D.i. Wei, Z. Liu, Carbon-Nanomaterial-Based Flexible Batteries for Wearable Electronics, Adv. Mater. 31 (9) (2019) 1800716.
[2] T. Tao, S. Lu, Y. Chen, A Review of Advanced Flexible Lithium-Ion Batteries, Adv. Mater. Technol. 3 (9) (2018) 1700375.
[3] H. Cha, J. Kim, Y. Lee, J. Cho, M. Park, Issues and Challenges Facing Flexible Lithium-Ion Batteries for Practical Application, Small 14 (43) (2018) 1702989.
[4] B. Yao, J. Zhang, T. Kou, Y.u. Song, T. Liu, Y. Li, Yat Li, Paper-Based Electrodes for Flexible Energy Storage Devices, Adv. Sci. 4 (7) (2017) 1700107.
[5] Z. Chen, J.W.F. To, C. Wang, Z. Lu, N. Liu, A. Chortos, L. Pan, F. Wei, Y.i. Cui, Z. Bao, A Three-Dimensionally Interconnected Carbon Nanotube-Conducting Polymer Hydrogel Network for High Performance Flexible Battery Electrodes, Adv. Energy Mater. 4 (12) (2014) 1400207, https://doi.org/10.1002/aenm.201400207.
[6] Z. Karam, R.A. Susantyoko, A. Alhammadi, I. Mustafa, C.H. Wu, S. Almheiri, Development of Surface-Engineered Tape-Casting Method for Fabricating Freestanding Carbon Nanotube Sheets Containing Fe$_2$O$_3$ Nanoparticles for Flexible Batteries, Adv. Eng. Mater. 1701019 (2018).
[7] Y. Zhang, Y. Li, Y. Wang, R. Guo, W. Liu, H. Pei, G. Yin, D. Ye, S. Yu, J. Xie, A flexible copper sulfide@multi-walled carbon nanotubes cathode for advanced magnesium-lithium-ion batteries, J. Colloid Interf. Sci. 553 (2019) 239–246.
[8] Y. Wang, Z.-y. He, Y.-X. Wang, C. Fan, C.-R.-L. Liu, Q.-l. Peng, J.-j. Chen, Z.-S. Feng, Preparation and characterization of flexible lithium iron phosphate/graphene/cellulose electrode for lithium ion batteries, J. Colloid Interf. Sci. 512 (2018) 398–403.
[9] B. Zhu, X. Wang, P. Yao, J. Li, J. Zhu, Towards high energy density lithium battery anodes: silicon and lithium, Chem. Sci. 10 (30) (2019) 7132–7148.
[10] C. Xie, Q. Xu, H. Maleki Kheimeh Sari, X. Li, Elastic buffer structured Si/C microsphere anodes via polymerization-induced colloid aggregation, Chem. Commun. 56 (50) (2020) 6770–6773.
[11] Q. Yang, Z. Wang, Y. Xia, G. Wu, C. Chen, J. Wang, P. Rao, A. Dong, Facile electrostatic assembly of Si@MXene superstructures for enhanced lithium-ion storage, J. Colloid Interf. Sci. 580 (2020) 68–76.
[12] T. Mu, S. Lou, N.G. Holmes, C. Wang, M. He, B. Shen, X. Lin, P. Zuo, Y. Ma, R. Li, C. Du, J. Wang, G. Yin, X. Sun, Reversible Silicon Anodes with Long Cycles by Multifunctional Volumetric Buffer Layers, ACS Appl. Mater. Interfaces 13 (3) (2021) 4093–4101.
[13] W. Lu, X. Zhou, Y. Liu, L. Zhu, Crack-Free Silicon Monoxide as Anodes for Lithium-Ion Batteries, ACS Appl. Mater. Interfaces 12 (51) (2020) 57141–57145.
[14] F. Xi, Z. Zhang, X. Wan, S. Li, W. Ma, X. Chen, R. Chen, B. Luo, L. Wang, High-Performance Porous Silicon/Nanosilver Anodes from Industrial Low-Grade Silicon for Lithium-Ion Batteries, ACS Appl. Mater. Interfaces 12 (43) (2020) 49080–49089.
[15] S. Chae, S.H. Choi, N. Kim, J. Sung, J. Cho, Integration of Graphite and Silicon Anodes for the Commercialization of High-Energy Lithium-Ion Batteries, Angew. Chem. Int. Ed. 59 (2020) 110–135.
[16] V.A. Davis, A.N.G. Parra-Vasquez, M.J. Green, P.K. Rai, N. Behabtu, V. Prieto, R.D. Booker, J. Schmidt, E. Kesselman, W. Zhou, H. Fan, W.W. Adams, R.H. Hauge, J.E. Fischer, Y. Cohen, Y. Talmon, R.E. Smalley, M. Pasquali, True solutions of single-walled carbon nanotubes for assembly into macroscopic material, Nature Nanotechnol. 4 (2009) 830–834.
[17] N. Behabtu, C.C. Young, D.E. Tsentalovich, O. Kleinerman, X. Wang, A.W.K. Ma, E.A. Bengio, R.F. ter Waarbeek, J.J. de Jong, R.E. Hoogerwerf, S.B. Fairchild, J.B. Ferguson, B. Maruyama, J. Kono, Y. Talmon, Y. Cohen, M.J. Otto, M. Pasquali, Strong, Light, Multifunctional Fibers of Carbon Nanotubes with Ultrahigh Conductivity, Science 339 (6116) (2013) 182–186.
[18] C.M. Niu, C. Xie, Y.H. Cheng, Non-metallic light conductive wire and its method and application products, US patent, US 9934881 B2.
[19] C. Xie, S. Yang, J.-W. Shi, X. Li, C. Niu, A double-walled carbon nanotubes conducting wire prepared by dip-coating, Mater. Res. Express 6 (9) (2019) 0950b7, https://doi.org/10.1088/2053-1591/ab0f62.
[20] F. Mirri, N.D. Orloff, A.M. Forster, R. Ashkar, R.J. Headrick, E.A. Bengio, C.J. Long, A. Choi, Y. Luo, A.R. Hight Walker, P. Butler, K.B. Migler, M. Pasquali, Lightweight, Flexible, High-Performance Carbon Nanotube Cables Made by Scalable Flow Coating, ACS Appl. Mater. Inter. 8 (7) (2016) 4903–4910.

[21] F. Villalpando-Paez, H. Son, D. Nezich, Y.P. Hsieh, J. Kong, Y.A. Kim, D. Shimamoto, H. Muramatsu, T. Hayashi, M. Endo, M. Terrones, M.S. Dresselhaus, Raman Spectroscopy Study of Isolated Double-Walled Carbon Nanotubes with Different Metallic and Semiconducting Configurations, Nano Lett. 8 (11) (2008) 3879–3886.

[22] R. Zhang, Y. Zhang, Q. Zhang, H. Xie, W. Qian, F. Wei, Growth of Half-Meter Long Carbon Nanotubes Based on Schulz-Flory Distribution, ACS Nano 7 (7) (2013) 6156–6161.

[23] X. Chen, H.X. Li, Z.H. Yan, F.Y. Cheng, J. Chen, Structure design and mechanism analysis of silicon anode for lithium-ion batteries, Sci. China Mater. 62 (2019) 1515–1536.

[24] B. Li, Y. Jiang, F. Jiang, D. Cao, H. Wang, C. Niu, Bird's nest-like nanographene shell encapsulated Si nanoparticles: Their structural and Li anode properties, J. Power Sources 341 (2017) 46–52.

[25] Y. Jiang, H. Wang, B. Li, Y.i. Zhang, C. Xie, J. Zhang, G. Chen, C. Niu, Interfacial engineering of Si/multi-walled carbon nanotube nanocomposites towards enhanced lithium storage performance, Carbon 107 (2016) 600–606.

[26] C. Meier, S. Lüttjohann, V.G. Kravets, H. Nienhaus, A. Lorke, H. Wiggers, Raman properties of silicon nanoparticles, Phys. E 32 (1-2) (2006) 155–158.

[27] J.J. Vilatela, J.A. Elliott, A.H. Windle, A model for the strength of yarn-like carbon nanotube fibers, ACS Nano 5 (3) (2011) 1921–1927.

[28] G. Qian, X. Liao, Y. Zhu, F. Pan, X.i. Chen, Y. Yang, Designing Flexible Lithium-Ion Batteries by Structural Engineering, ACS Energy Lett. 4 (3) (2019) 690–701.

[29] P. Li, J.Y. Hwang, Y.K. Sun, Nano/Micro-Structured Silicon-Graphite Composite Anode for High-Energy Density Li-Ion Battery, ACS Nano 13 (2019) 2624–2633.

[30] V. Augustyn, J. Come, M.A. Lowe, J.W. Kim, P.-L. Taberna, S.H. Tolbert, H.D. Abruña, P. Simon, B. Dunn, High-rate electrochemical energy storage through Li$^+$ intercalation pseudocapacitance, Nat. Mater. 12 (6) (2013) 518–522.

[31] M. Yousaf, Y.J. Chen, H. Tabassum, Z.P. Wang, Y.S. Wang, A.Y. Abid, A. Mahmood, N. Mahmood, S.J. Guo, R.P.S. Han, P. Gao, A Dual Protection System for Heterostructured 3D CNT/CoSe$_2$/C as High Areal Capacity Anode for Sodium Storage, Adv. Sci. 7 (2020) 1902907.

[32] A.M. Gaikwad, B.V. Khau, G. Davies, B. Hertzberg, D.A. Steingart, A.C. Arias, A High Areal Capacity Flexible Lithium-Ion Battery with a Strain-Compliant Design, Adv. Energy Mater. 5 (3) (2015) 1401389, https://doi.org/10.1002/aenm.201401389.

[33] J.Y. Wang, L. Liao, Y.Z. Li, J. Zhao, F.F. Shi, K. Yan, A. Pei, G.X. Chen, Z.Y.L. Guodong Li, Y. Cui, Shell-Protective Secondary Silicon Nanostructures as Pressure Resistant High-Volumetric-Capacity Anodes for Lithium-Ion Batteries, Nano Lett. 18 (2018) 7060–7065.

[34] Y. Shang, C. Wang, X. He, J. Li, Q. Peng, E. Shi, R. Wang, S. Du, A. Cao, Y. Li, Self-stretchable, helical carbon nanotube yarn supercapacitors with stable performance under extreme deformation conditions, Nano Energy 12 (2015) 401–409.

[35] K. Wang, S. Luo, Y. Wu, X.F. He, F. Zhao, J.P. Wang, K.L. Jiang, S.S. Fan, Super-Aligned Carbon Nanotube Films as Current Collectors for Lightweight and Flexible Lithium Ion Batteries, Adv. Funct. Mater. 23 (2013) 846–853.

[36] E. Qu, T. Chen, Q. Xiao, G. Lei, Z. Li, Freestanding silicon/carbon nanofibers composite membrane as a flexible anode for Li-Ion battery, J. Power Source 403 (2018) 103–108.

[37] H.W. Wang, J.Z. Fu, C. Wang, J.Y. Wang, A.K. Yang, C.C. Li, Q.F. Sun, Y. Cui, H.Q. Li, Binder-free High Silicon Content Flexible Anode for Li-ion Batteries, Energy Environ. Sci. 13 (2020) 848–858.

[38] S.-H. Park, P.J. King, R. Tian, C.S. Boland, J. Coelho, C. Zhang, P. McBean, N. McEvoy, M.P. Kremer, D. Daly, J.N. Coleman, V. Nicolosi, High areal capacity battery electrodes enabled by segregated nanotube networks, Nat. Energy 4 (7) (2019) 560–567.

[39] C.F. Zhang, S.H. Park, A. Seral-Ascaso, S. Barwich, N. McEvoy, C.S. Boland, J.N. Coleman, Y. Gogotsi, V. Nicolosi, High capacity silicon anodes enabled by MXene viscous aqueous ink, Nat. Commun. 10 (2019) 849.